JOURNAL OF THERMOPHYSICS AND HEAT TRANSFER
Vol. 11, No. 2, April–June 1997

Experiments and Analyses of Flat Miniature Heat Pipes

Y. Cao* and M. Gao†
Florida International University, Miami, Florida 33199
and
J. E. Beam‡ and B. Donovan§
U.S. Air Force Wright Laboratory, Wright–Patterson Air Force Base, Ohio 45433

Two flat copper–water axially grooved miniature heat pipes are fabricated employing the electric-discharge-machining (EDM) wire-cutting method. Because of the advantage of the EDM method, axial grooves are provided around the entire interior perimeters of the miniature heat pipes. The two miniature heat pipes are tested under different heat inputs, cooling temperatures, and orientations. The maximum heat transfer rate for the heat pipes tested is about 40 W, and the maximum heat flux achieved is about 20 W/cm^2, based on the outer surface of the evaporator. The effective thermal conductance of the heat pipe is on the order of 40 times that of copper based on the external cross-sectional area of the miniature heat pipe. If the effective thermal conductance is evaluated based on the interior cross-sectional area of the heat pipe, it can be 100 times higher than the thermal conductivity of copper. Analyses for heat-pipe limitations are also performed based on certain analytical relations. It is found that the capillary limit is the dominant heat transfer limitation for the miniature heat pipes tested in this paper. To improve the accuracy of the analytical model, the hydraulic radius in the capillary limit is corrected using the exact two-dimensional solutions found in the literature, and the expression for the friction factor that takes into account the shear stress at the liquid/vapor interface is adopted. The analytical results based on these modifications are compared with corresponding experimental results with good agreement.

Nomenclature

A = cross-sectional area, m^2
D_g = groove depth, m
$D_{l,h}$ = hydraulic diameter of the liquid groove, m
$D_{v,h}$ = hydraulic diameter of vapor space, m
F = frictional coefficient
f = skin-friction coefficient
H = height, m
h_{fg} = latent heat of evaporation, J/kg
K = permeability of the wick structure, m^2
K' = ratio of specific heats, c_p/c_v
k = thermal conductivity, W/m-K
$k_{w,e}$ = effective thermal conductivity of the wick structure, W/m-K
L = length of the heat pipe, m
N = number of grooves
p = pressure, N/m^2
Q = heat transfer rate, W
R_b = radius of vapor bubble, m
R_g = gas constant, J/kg-K
R_{men} = radius of the liquid–vapor meniscus, m
$Re_{l,h}$ = hydraulic liquid Reynolds number
$Re_{v,h}$ = hydraulic vapor Reynolds number
r = capillary radius of the wick pores, m
s = spacing, m
T = temperature, K
t_t = height of the curved top of fin, m
W, w = width, m
μ = dynamic viscosity, kg/m-s
ν = kinematic viscosity, m^2/s
ρ = density, kg/m^3
σ = surface tension, N/m
ε = porosity of the wick structure

Subscripts
a = adiabatic section
b = boiling heat transfer limit
c = condenser or coolant
ca = capillary
crit = critical
cu = copper
e = evaporation section
eff = effective
ent = entrainment heat transfer limit
g = groove, m
l = liquid phase
s = solid phase
son = sonic heat transfer limit
v = vapor

Received June 13, 1996; revision received Sept. 26, 1996; accepted for publication Sept. 30, 1996.

*Assistant Professor, Department of Mechanical Engineering.
†Research Coordinator, Department of Mechanical Engineering.
‡Deputy for Technology, Aerospace Power Division.
§Project Engineer, Aerospace Power Division.

Introduction

THERMAL management is one of the most critical technologies for electronic products and directly influences their cost, reliability, and performance. As power electronic devices become progressively smaller, while at the same time reliability issues drive down the parts required, each device is forced to handle more power. Consequently, the heat flux in electronic devices becomes increasingly higher, which makes heat dissipation difficult. To minimize the maximum junction temperature, a high thermal–conductive path is required. Micro/miniature heat pipes can be used to augment the thermal conductive path and spread the heat over a much larger surface area to reduce the high heat flux to a much smaller and manageable level.

The concept of the micro-heat pipe was first proposed by Cotter[1] with the application background of electronic cooling. Traditionally, if the hydraulic diameter of a heat pipe is on the order of 1 mm, it is referred to as a miniature heat pipe. For

a heat pipe with a hydraulic diameter on the order of 10 μm, it is considered to be a micro-heat pipe. A comprehensive review of micro-/miniature heat pipes and their limitations was given by Cao et al.[2] Detailed descriptions and modeling for micro-/miniature heat pipes can also be found in Faghri[3] and Khrustalev and Faghri.[4] Although micro-heat pipes have the advantages of being fabricated in extremely small sizes and the potential to be directly fabricated into silicon wafers, high heat-flux transportation is difficult to achieve because of the various heat transfer limitations. Miniature heat pipes, on the other hand, have the characteristics of conventional heat pipes and are capable of handling very high heat fluxes.

Babin et al.[5] tested a trapezoidal water heat pipe with a cross-sectional area of 1 mm^2 and a length of 57 mm. The maximum heat transfer rate was about 0.5 W. Wu and Peterson[6] tested a flat heat pipe with a cross section of 1 × 2 mm and a length of 60 mm, with water as the working fluid. A maximum heat transport rate of 1.3 W was obtained, which corresponds to a heat flux of 5 W/cm^2. Plesch et al.[7] tested two types of flat miniature heat pipes having overall dimensions of 7 (width) × 2 (thickness) × 120 (length) mm, with water as the working fluid. The first type of heat pipe has two arteries that are formed by the spars of an inserted frame and the wall of the casing. The transverse grooves were provided to allow the transverse transport of liquid working fluid in the heating and cooling zones. The second type, however, has longitudinal grooves over its entire length. For the first type, a maximum heat transport rate of about 16.5 W was obtained in a horizontal arrangement, with a wall temperature drop over the heat-pipe length of about 25°C. For the second type, the maximum heat transport rate was nearly 70 W with a temperature drop of about 35°C. It is clear from the large heat transport rate obtained by Plesch et al.[7] that small axial grooves are very effective in increasing the heat transfer capacity. Although they may be replaced by other wick structures such as sintered powders or screen wicks, the axial grooves have the advantages of eliminating the problems of low thermal conductivity and low permeability encountered in the screen wicks or sintered metal powder wicks. More importantly, axially grooved heat pipes feature integral structures for the shell and wick of the heat pipe. The objective of the present study is to develop axially grooved miniature heat pipes that have a large heat transport capacity and high effective thermal conductance. Two miniature heat pipes, with axial grooves provided around the entire perimeter, are fabricated, filled, and tested under different working conditions. Analytical predictions on heat transfer limitations are also made for the heat pipes.

Fabrication and Filling Procedures of the Miniature Heat Pipe

Two miniature heat pipe shells with axial grooves were fabricated by the electric-discharge-machining (EDM) wire-cutting method, which is a precise, noncontact machining technique. Any conductive material can be effectively machined to a high precision with a tolerance of ±0.0001 in., depending on the processing environment and the operator's skills. A minimum kerf width of 0.004 in. (less than that for the slow-speed wire EDM) and burr-free shells can be obtained using this method. Miniature heat pipes with various external shapes and axial grooves can be fabricated for a different application. Therefore, this method is very useful for studying the heat transfer characteristics of miniature heat pipes. The configurations and dimensions of the two miniature heat pipes fabricated are shown in Fig. 1 in terms of the overall dimensions and the cross-sectional dimensions. Because the miniature heat pipe has a very small interior space, filling the heat pipe presents one of the greatest challenges. In this study, an injection-charging method was used for the filling purpose. The filling assembly is schematically shown in Fig. 2, which includes a tubular adapter and a vacuum system. An electrical heater and five thermocouples were attached along the heat-pipe length.

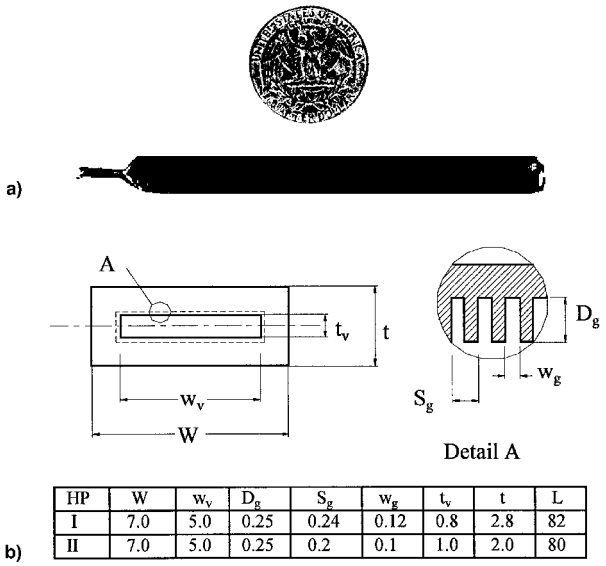

b)

HP	W	w_v	D_g	S_g	w_g	t_v	t	L
I	7.0	5.0	0.25	0.24	0.12	0.8	2.8	82
II	7.0	5.0	0.25	0.2	0.1	1.0	2.0	80

Fig. 1 Samples of miniature heat pipes: a) overall dimensions and b) cross section dimensions in millimeters.

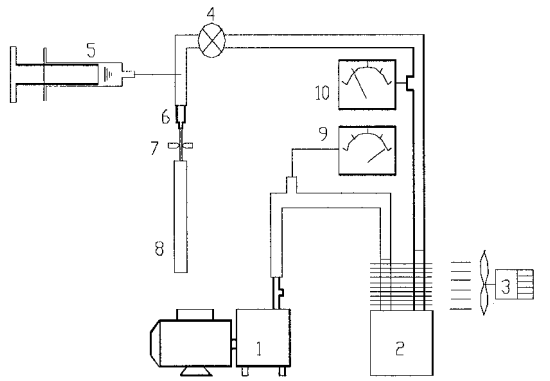

Fig. 2 Working fluid filling system: 1, vacuum pump; 2, diffusion pump; 3, cooling fan; 4, valve; 5, syringe; 6, adapter; 7, vise grip; 8, heat pipe; 9, low-vacuum gauge; and 10, high-vacuum gauge.

A filling tube (tempered oxygen-free copper with a 1/16 in. o.d.) was attached to the end-cap of the miniature heat pipe. The heat pipe was evacuated at its designed working temperature to a pressure of 8 × 10^{-4} torr (10^{-7} torr could be achieved if the evacuation process was held for 24 h for the elimination of gas molecules on the inside grooved wall). After the desired vacuum condition was achieved, the valve next to the filling tube on the vacuum hose was closed, and an amount of water was injected into the heat pipe through the vacuum hose using a scaled syringe. Excessive working fluid was needed because some working fluid could stick to the inner walls of the hose and tube adapter. The heat pipe was then heated to over 100°C until the axial temperature distribution became uniform. It was then sealed by pinching the filling tube off and soldering the end. It should be pointed out that an accurate control of the working fluid charge was impossible through this method because of the large surface areas of the vacuum hose and adapter, compared to the internal surface area of the miniature heat pipe itself. However, it was believed that, when the heat pipe was heated up and the axial temperatures became uniform, the excessive fluid was swept out of the heat pipe by the vapor flow, leaving an appropriate amount of working fluid in the heat-pipe wick structure.

Experimental Apparatus

The experimental apparatus for miniature heat-pipe testing is shown schematically in Fig. 3 and consists of a constant

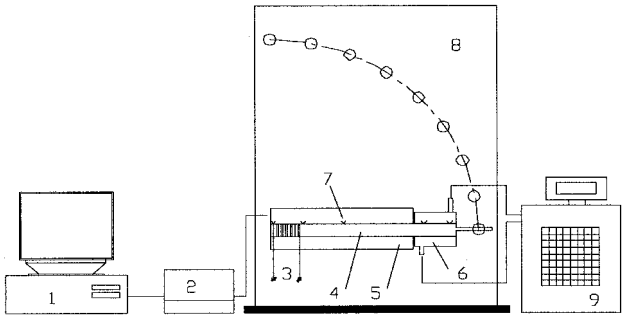

Fig. 3 Schematic of test apparatus: 1, computer; 2, scanning thermocouple thermometer; 3, electrical heater; 4, heat pipe; 5, thermal insulation; 6, cooling jacket; 7, thermocouples; 8, angulometer; and 9, constant temperature circulator.

temperature circulator, a transformer, a scanning thermocouple thermometer, and a computer. Stainless-steel wires, 0.1-mm-diam, were wound around the evaporator section to supply heat to the heat pipe. Between the heater and the heat-pipe surface was a layer of 0.05-mm Kapton electric insulation. Both the evaporator and adiabatic sections were thermally insulated with asbestos paper. The power input Q to the heater was controlled through a variable transformer and measured with a digital multimeter. The heat loss from the insulation surface to the ambient was determined by evaluating the temperature difference and the heat transfer coefficient of natural convection between the insulated outer surface and ambient. Within the test range the maximum heat loss was less than 0.3 W and was therefore negligible. For heat pipe no. 1, the evaporator and condenser lengths were 19 and 20 mm, respectively. For heat pipe no. 2, both evaporator and condenser lengths were 10 mm. The condenser section of the heat pipe was placed in a water-cooling jacket that was connected to a constant temperature circulator. The circulator could be set at any desired temperature and flow rate. Five type-K (NiCr–NiAl) precision fine-wire thermocouples, 0.127-mm-diam, were installed along the heat-pipe length to measure the surface temperature distribution. To secure the contact between the heat pipe and the thermocouples, the thermocouples were soldered onto the heat-pipe wall. The thermocouples were located, respectively, at 3, 28, 41, 70, and 80 mm from the endcap of the evaporator section for miniature heat pipe No. 1. For heat pipe No. 2, the thermocouples were located at 3, 13, 40, 73, and 78 mm from the evaporator end-cap. The temperature data were taken using the 12-channel scanning thermocouple thermometer and were transferred to the computer through the serial port. The thermometer features the field calibration for each channel to eliminate the error of the thermocouple probes and the system for precise measurement. When the steady state of the heat pipe was achieved during the testing process, the average value of 10 readings was recorded as the final experimental result to further reduce the error. Within the test range, the error was less than 1%, for temperature measurement, and 2% for power measurement. The test procedures include changing the power inputs to the heat pipe and the temperature of cooling water.

Results

Figures 4–8 present some representative testing results for heat pipe no. 1 in terms of temperature distribution along the heat pipe length and the ratio of the heat-pipe effective thermal conductance to copper thermal conductivity. The effective thermal conductance of the heat pipe was calculated by $K_{\text{eff}} = QL/[A(T_1 - T_2)]$, where A is the cross-sectional area of the heat pipe, and T_1 and T_2 are temperatures at the evaporator and condenser end-caps. The copper thermal conductivity in the figures is taken to be 380 W/m-K. The experiments were undertaken at different coolant temperatures T_c through the adjustment of the coolant bath temperature. At each cooling temperature, the power input to the heat pipe was gradually increased from a lower level to a higher level until the temperature drop across the heat-pipe length reached about 20–25°C. It should be pointed out that the heat pipe was still able to work steadily at this range of temperature drops. However, it was believed that the dryout at the evaporator end-cap had occurred and the surface of evaporation had shifted toward the middle section of the heat pipe. Also, the effective thermal conductance of the heat pipe had decreased to a fairly low level. Therefore, it was determined that the heat transfer limit had been reached when the temperature drop exceeded 20–25°C, and the experiment testing was terminated. The experimental results show that the heat transfer limit is largely dependent on the working temperature level. The heat transfer limit was increased from about 20 W at a coolant temperature of 70°C to 31 W at the coolant temperature of 90°C, which corresponds to a heat flux of about 14 W/cm^2, based on the evaporator surface area. The increase in the heat-pipe capacity as the working temperature increases is attributable to the decrease in liquid viscosity, which subsequently reduces the flow resistance and increases the heat transfer limitation. For the experimental results shown in Fig. 4, it was obvious that the heat transfer limitation had not been reached. The testing at

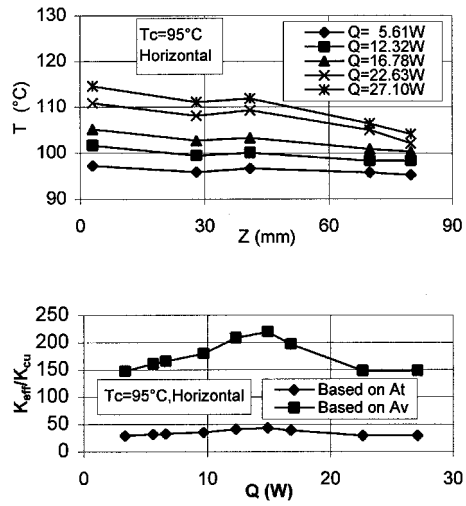

Fig. 4 Experimental results of heat pipe no. 1 for coolant temperature of 95°C.

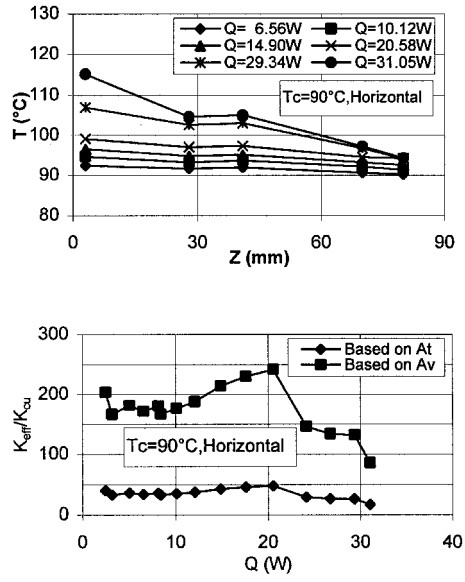

Fig. 5 Experimental results of heat pipe no. 1 for coolant temperature of 90°C.

this coolant temperature was terminated because of the large evaporation rate of the cooling water in the circulating bath at this elevated temperature. The effective thermal conductance of the heat pipe was presented based on both external cross-sectional area, A_t and the cross-sectional area of the vapor space A_v. The thickness of the heat-pipe shell was deliberately made larger for the consideration of heat-pipe sealing and strength. To more accurately judge the performance of the heat pipe, the effects of the shell may be excluded. As can be seen from the figures, the ratio of the heat-pipe effective thermal conductance to copper thermal conductivity is on the order of 100, based on the vapor space cross-sectional area, compared to 40–50 based on the external cross-sectional area. Figure 9 shows the experimental results at the coolant temperature of 90°C when the heat pipe was placed in a vertical orientation. The heat transfer was significantly enhanced because of the reflux working conditions in the heat pipe. Even at a heat input of 45 W, the heat pipe still worked normally.

Figures 10–13 present testing results for heat pipe no. 2 at different coolant temperatures and heat inputs. The evaporator and condenser lengths for this heat pipe were both 10 mm, which were much shorter than those of heat pipe no. 1. The heat flux at the evaporator was about 20.6 W/cm^2 based on the evaporator surface area, at a power input of 24.8 W and coolant temperature of 90°C for the testing results presented in Fig. 10. The temperature drop at the evaporator was much steeper compared to that of heat pipe no. 1 because of this higher heat flux. The temperature readings of thermocouple no. 4 in the condenser section were abnormally low and were always closed to the coolant temperature. It was believed that the thermocouple was somehow exposed to the coolant, and the temperature reading at that point was disregarded when evaluating the heat-pipe performance.

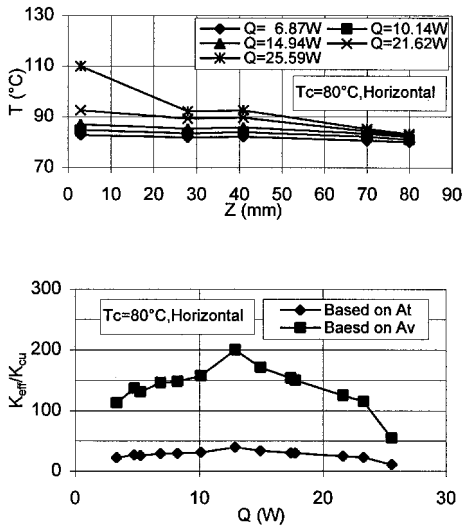

Fig. 6 Experimental results of heat pipe no. 1 for coolant temperature of 80°C.

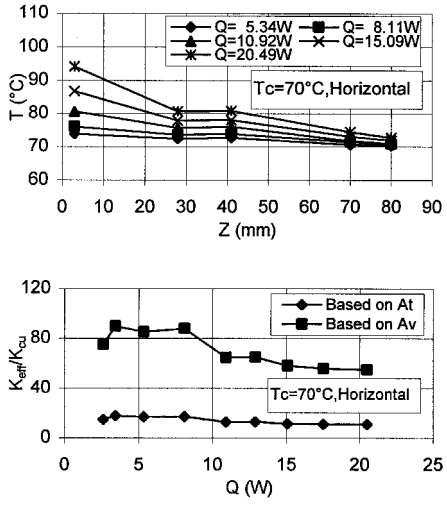

Fig. 7 Experimental results of heat pipe no. 1 for coolant temperature of 70°C.

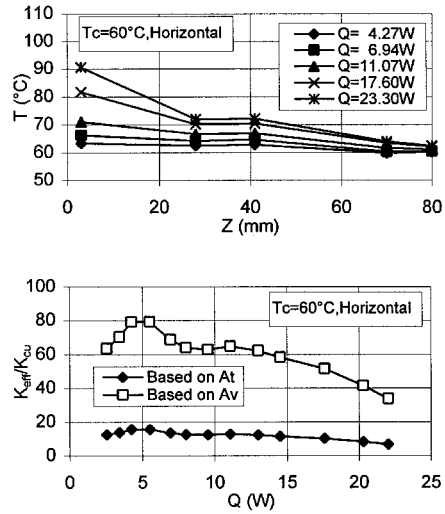

Fig. 8 Experimental results of heat pipe no. 1 for coolant temperature of 60°C.

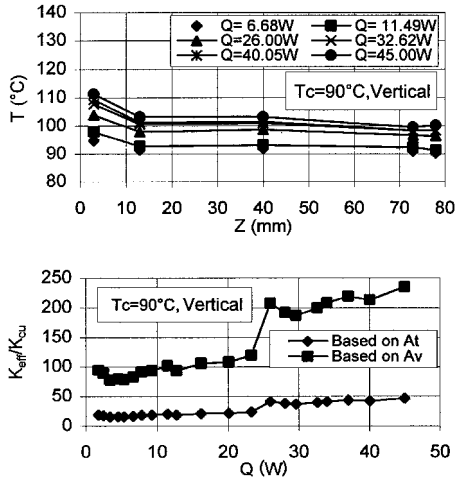

Fig. 9 Experimental results of heat pipe no. 1 in vertical arrangement.

Analyses of the Heat Transfer Limitations

The analyses of the heat transfer limitations for miniature heat pipes are based on some analytical relations from Faghri,[3] with some important modifications. The most important heat transfer limitations for the present miniature heat-pipe applications are capillary, boiling, entrainment, and sonic limitations. The capillary limit can be evaluated using the following equation:

$$Q_{c_{ap}} = \frac{2\sigma/r_{\text{eff}}}{(F_l + F_v)L_{\text{eff}}} \tag{1}$$

where r_{eff} is the effective pore radius of the wick structure. For the present axial grooves, r_{eff} is equal to the groove width w_g, and L_{eff} is the effective length of the heat pipe, which is equal

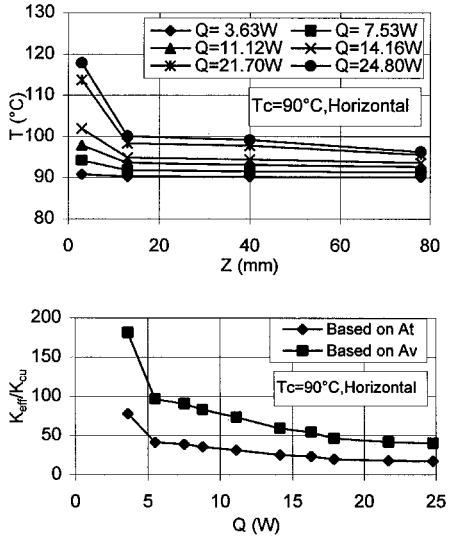

Fig. 10 Experimental results of heat pipe no. 2 for coolant temperature of 90°C.

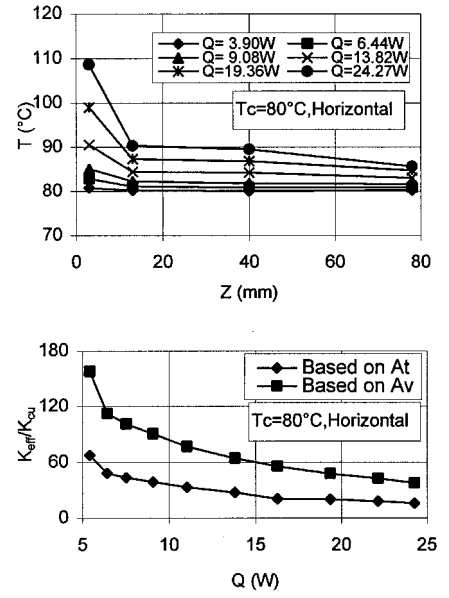

Fig. 11 Experimental results of heat pipe no. 2 for coolant temperature of 80°C.

to $L_a + 0.5(L_e + L_c)$. The liquid and vapor frictional coefficients are defined, respectively, as the following:

$$F_l = \frac{\mu}{\rho_l A_w K h_{fg}} \tag{2}$$

$$F_v = \frac{(fRe_{v,h})\mu_v}{2\pi R_{v,h}^4 \rho_v h_{fg}} \tag{3}$$

where A_w is the cross-sectional area of the wick structure. For the axially grooved wick structure

$$K = \frac{D_{l,h}^2 \varsigma}{2(fRe_{l,h})} \tag{4}$$

where ς can be evaluated by $\varsigma = w_g/s_g$. The hydraulic diameter for the vapor flow space $D_{v,h} = 2R_{v,h}$, and that of the axially

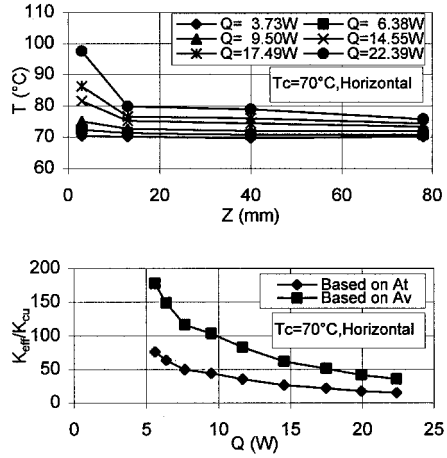

Fig. 12 Experimental results of heat pipe no. 2 for coolant temperature of 70°C.

grooved wick structure $D_{l,h}$, can be evaluated, respectively, by the following relations:

$$D_{v,h} = 2t_v w_v/(t_v + w_v) \tag{5}$$

$$D_{l,h} = 4D_g w_g/(2D_g + w_g) \tag{6}$$

The expression for $fRe_{v,h}$ can be found in Faghri[3] for the present noncircular vapor flow space:

$$fRe_{v,h} = 24(1 - 1.355\alpha + 1.947\alpha^2 - 1.701\alpha^3 + 0.956\alpha^4 - 0.254\alpha^5) \tag{7}$$

where $\alpha = w_v/t_v$, when $w_v < t_v$ or $\alpha = t_v/w_v$, when $w_v > t_v$.

For $fRe_{l,h}$, the relation from Schneider and Devos[8] is used to take into account the shear stress in the liquid at the interface caused by the liquid/vapor frictional interaction. The same equation was used by Khrustalev et al.[9] in their numerical modeling on axially grooved heat pipes, with good agreement between their numerical results and experimental data in the literature:

$$fRe_{l,h} = (fRe_{l,h})_0 \left(1 + \frac{Nw_g^3}{6\pi D_{v,h}^3}(fRe_{v,h})\frac{\nu_v}{\nu_l} \times \left\{1 - 1.971 \exp\left[-\frac{\pi(D_g - t_t)}{w_g}\right]\right\}\right) \tag{8}$$

where t_t is the height of the curved top of the fin, which is zero in the present case. $(fRe_{l,h})_0$ corresponds to the case with no liquid–vapor interaction, which can be evaluated using the following relation:

$$(fRe_{l,h})_0 = 8(D_g - t_g)^2 \left\{\frac{w_g^2}{4}\left[1 + \frac{2(D_g - t_t)}{w_g}\right]^2 \times \left(\frac{1}{3} - \frac{32w_g}{\pi^5(D_g - t_t)}\tanh\left[\frac{\pi(D_g - t_t)}{w_g}\right]\right)\right\}^{-1} \tag{9}$$

The boiling limitation can be evaluated based on the relation from Cao and Faghri.[10] The critical superheat for the boiling in the wick structure is

$$\Delta T_{crit} = \frac{R_g T_v^2}{h_{fg}} \ell n \left[1 + \frac{2\sigma}{p_v}\left(\frac{1}{R_b} - \frac{1}{R_{men}}\right) + \frac{2\sigma\rho_v}{p_v R_b p_l}\right] \tag{10}$$

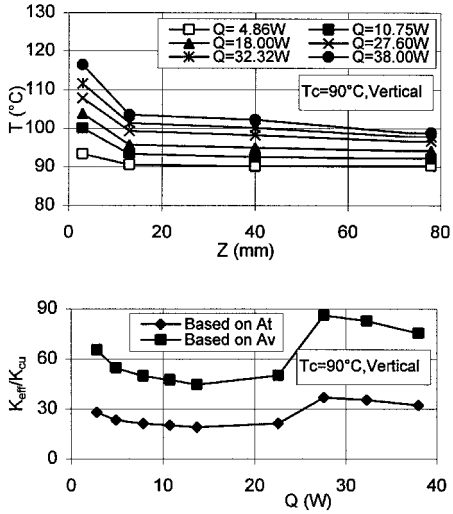

Fig. 13 Experimental results of heat pipe no. 2 in vertical arrangement.

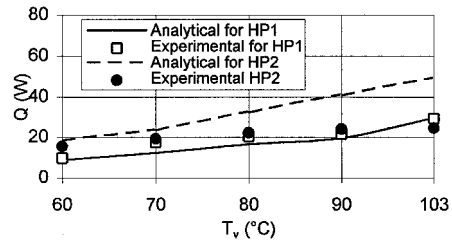

Fig. 14 Comparison of analytical predictions and experimental data for the heat transfer limit.

The boiling limitation associated with the critical superheat is therefore

$$Q_b = 2(w_v + t_v)L_e k_{w,e}(\Delta T_{crit}/D_g) \tag{11}$$

The effective thermal conductivity of the wick structure in the previous equation can be estimated using the following equation[3]:

$$k_{w,e} = \frac{(s_g - w_g)k_l k_s D_g + w_g k_l[0.185(s_g - w_g)k_s + D_g k_l]}{s_g[0.185(s_g - w_g)k_s + D_g k_l]} \tag{12}$$

The entrainment heat transfer limitation can be calculated by the equation[3]

$$Q_{ent} = A_v h_{fg}(\sigma\rho_v/2w_g)^{0.5} \tag{13}$$

where A_v is the cross-sectional area of the heat-pipe vapor space. Finally, the sonic limitation can be evaluated by the equation[3]

$$Q_{son} = A_v \rho_0 h_{fg}\left[\frac{K' R_g T_0}{2(K'+1)}\right]^{0.5} \tag{14}$$

where ρ_0 and T_0 are the vapor density and temperature at the evaporator end-cap.

The various potential heat transfer limitations presented earlier were evaluated for the two miniature heat pipes. It was found that the actual heat transfer limit was always the capillary limit for these two heat pipes. The capillary limits predicted by Eqs. (1–9) are compared with the corresponding experimental data in Fig. 14. The operating temperature T_v in the figure is the temperature at the adiabatic section of the heat pipe. The agreement between the analytical and experimental results is excellent for heat pipe no. 1. The agreement for heat pipe no. 2, however, is less favorable, especially at a higher operating temperature. Such discrepancy may be caused by the uncertainty in the groove dimensions of the heat pipe. Heat pipe no. 2 was cleaned using a relatively strong acid solution. It was believed that the groove width was somehow increased because of this cleaning process. It is also important to note that the formulation of the capillary limitation is based on the concept of the hydraulic diameter. Because the vapor flow in the heat pipe is laminar, a large percent error may be involved for a rectangular cross section of vapor space having a large slenderness ratio. To improve the accuracy of the analytical prediction, the hydraulic diameter for the rectangular vapor space in Eq. (5) was corrected in this paper using the exact two-dimensional relations from White.[11]

Conclusions

Two flat miniature heat pipes were fabricated employing the EDM wire-cutting method. The fabricated miniature heat pipes have been tested under various working conditions. The testing results indicated that the heat pipes worked very well at relatively high power inputs. The maximum heat input and heat flux at the evaporator were about 31 W and 20.6 W/cm^2, respectively, for the horizontal arrangement. The effective thermal conductance of the heat pipe was on the order of 40 times that of copper based on the external cross-sectional area of the miniature heat pipe.

Heat transfer limitations were predicted for the two miniature heat pipes by employing some analytical relations. The analytical results agreed very well with experimental results for heat pipe no. 1. The agreement was less satisfactory for heat pipe no. 2 because of the uncertainties in wick structure dimensions. To improve the accuracy of the analytical prediction, it is very important that the hydraulic radius in the capillary limit be corrected using the exact two-dimensional solutions, and the expression for the friction factor that takes into account the shear stress at the liquid/vapor interface be adopted. It should be pointed out that the dimensions of the two miniature heat pipes tested in this paper are not optimal. Research work is continuing for the optimization of the heat-pipe design in an effort to further increase the heat transfer capacity of the miniature heat pipe.

Acknowledgments

This work was sponsored by BMDO's Innovative Science and Technology Office and managed by the U.S. Air Force Wright Laboratory.

References

[1]Cotter, T. P., "Principles and Properties of Micro Heat Pipes," *Proceedings of the 5th International Heat Pipe Conference* (Tsukuba, Japan), 1984, pp. 328–335.

[2]Cao, Y., Faghri, A., and Mahefkey, T., "Micro/Miniature Heat Pipes and Operating Limitations," American Society of Mechanical Engineers, HTD-Vol. 236, 1993, pp. 55–62.

[3]Faghri, A., *Heat Pipe Science and Technology*, Taylor and Francis, Washington, DC, 1995.

[4]Khrustalev, D. K., and Faghri, A., "Thermal Analysis of a Micro Heat Pipe," *Journal of Heat Transfer*, Vol. 116, No. 1, 1994, pp. 189–198.

[5]Babin, B. R., Peterson, G. P., and Wu, D., "Steady-State Modeling and Testing of a Micro Heat Pipe," *Journal of Heat Transfer*, Vol. 112, Aug. 1990, pp. 595–601.

[6]Wu, D., and Peterson, G., "Experimental Investigation of the Transient Behavior of Micro Heat Pipes," *Proceedings of the AIAA/ASME 5th Joint Thermophysics and Heat Transfer Conference* (Seattle, WA), AIAA, Washington, DC, 1990.

[7]Plesch, D., Bier, W., Seidel, D., and Schubert, K., "Miniature

Heat Pipes for Heat Removal from Microelectronic Circuits,'' American Society of Mechanical Engineers, DSC-Vol. 32, 1991, pp. 303–313.

[8]Schneider, G. E., and Devos, R., ''Nondimensional Analysis for the Heat Transport Capillary of Axially-Grooved Heat Pipes Including Liquid/Vapor Interaction,'' AIAA Paper 80-0214, Jan. 1980.

[9]Khrustalev, D. K., and Faghri, A., ''Heat Transfer During Evaporation and Condensation on Capillary-Grooved Structures of Heat Pipes,'' *Proceedings of the ASME Winter Annular Meeting*, Chicago, IL, 1994.

[10]Cao, Y., and Faghri, A., ''Analysis of Transient and Steady-State Performances of Nosecap and Wing Leading Edge Heat Pipes,'' HTD-Vol. 221, American Society of Mechanical Engineers, New York, 1992, pp. 43–52.

[11]White, F. M., *Viscous Fluid Flow*, McGraw–Hill, New York, 1974.